JOURNAL OF GEOPHYSICAL RESEARCH, VOL. 100, NO. A10, PAGES 19,329–19,342, OCTOBER 1, 1995

A storm time assimilative mapping of ionospheric electrodynamics analysis for the severe geomagnetic storm of November 8-9, 1991

M. L. Cooper and C. R. Clauer
Space Physics Research Laboratory, University of Michigan, Ann Arbor

B. A. Emery and A. D. Richmond
National Center for Atmospheric Research, Boulder, Colorado

J. D. Winningham
Southwestern Research Institute, San Antonio, Texas

Abstract. Global parameters are obtained for the November 8-9, 1991 severe geomagnetic storm with the application of a slightly modified version of the Assimilative Mapping of Ionospheric Electrodynamics (AMIE) data inversion model. Inputs to the model include ground magnetometer data, satellite electron precipitation data, satellite ion drift data, and ion drift velocities obtained from radar measurements. We compare two of the AMIE computed parameters, the total Joule heating and the polar cap potential, to both the $AE(12)$ index and the AE_{AMIE} index, an AMIE modeled AE index created specifically for severe storm times. The equation obtained from a linear fit to the total Joule heating versus the AE_{AMIE} index closely resembles other equations found during much less disturbed times using the $AE(12)$ index. Our results using the $AE(12)$ index appear to saturate at a level around 1300 nT. However, this saturation is associated with the calculation of the $AE(12)$ index and not a physical result. An apparent saturation can also be seen in our comparison of the polar cap potential with the $AE(12)$ index, but this is not the case when using the AE_{AMIE} index. The comparison between the polar cap potential and the AE_{AMIE} index yields an approximate linear relationship with a correlation coefficient of 0.80. From our results, we find that the magnitude of the auroral electrojets and the polar cap potential drop do not show signs of saturation at the activity levels that were present during the November 8-9, 1991 severe storm.

Introduction

A magnetic storm is a disturbance at low and midlatitudes during which the Earth's magnetic field is depressed by a westward flowing ring current in the magnetosphere and the auroral electrojets are observed at lower than normal latitudes. The worldwide magnetic disturbance produced during magnetic storms is generally characterized through the use of various magnetic indices. These indices include the K_p, a_p, A_p, and Dst indices. The K_p index is a value between 0 and 9 assigned to a certain level of disturbance according to the observed global fluctuations in the magnetic field during a 3-hour interval of universal time (UT). The K_p index is based on a quasi-logarithmic scale described in detail by *Rostoker* [1972]. A representation of this index using a linear scale is given by the a_p index. The a_p index can be interpreted as the equivalent amplitude of a disturbance at a standard midlatitude station in units of 2 nT [*Rostoker*, 1972]. The value of a_p ranges from 0 to 400 and the daily average calculated in universal time is the more commonly known A_p index. *Dst* is the hourly measure of the globally averaged low-latitude horizontal component of the Earth's magnetic field.

There are three classifications of magnetic storms: minor, major, and severe. According to the World Data Center in Boulder, Colorado (personal communication, 1994), this classification can depend upon either the K_p or A_p indices. Minor storms have a K_p of 5 and an A_p index between 30 and 50, major storms have a K_p of 6 and an A_p index between 50 and 100, and severe storms have a K_p of 7, 8, or 9 and an A_p index of 100 or more.

The onset of the storm that occurred during the interval of November 8-9, 1991, is marked by a sudden commencement occurring around 1400 UT November 8.

Paper number 95JA01402.
0148-0227/95/95JA-01402$05.00

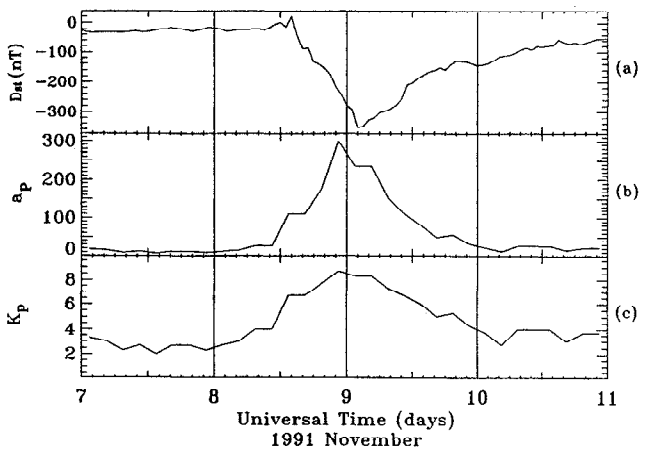

Figure 1. Some standard geophysical indices for the November 8 and 9, 1991 severe geomagnetic storm: (a) *Dst* index, (b) the 3-hour a_p index, and (c) the 3-hour K_p index.

The K_p index reached a maximum value of 9− at 2230 UT November 8 and sustained a value of 8± for the next 6 hours, indicating a severe storm. The K_p index for this period is shown in Figure 1 along with the *Dst* and a_p indices. The *Dst* index has also been used in classifying magnetic activity where severe storms would have a "peak" *Dst* of −100 nT or less. Figure 1 shows that soon after the peak activity of the storm the *Dst* has plummeted to a value of −354 nT. The decline in *Dst* is generally called the main phase of the storm, which develops due to a sustained, southward Interplanetary Magnetic Field (IMF).

Figure 1 shows that the a_p index peaks around 2230 UT on November 8. Since the peak a_p occurs almost at the end of the first day of this 2-day storm, we get a better indication of the strength of the storm by creating a "daily" A_p which is averaged over an interval that better represents the actual storm period. Averaging the a_p index from 1330 UT November 8 to 1030 UT November 9 gives a daily A_p index of 180 which is well above the value indicating a severe storm.

The duration of magnetic storms can be of the order of several hours to over a day. The exact time seems to depend upon the length of time that the Z component of the IMF is negative (southward), the magnitude that it maintains, and the length of time that it takes for the magnetosphere-ionosphere system to recover. The location of the auroral oval is typically around 68° magnetic latitude on the nightside and 75° on the dayside. However, during storm conditions, the auroral oval brightens (intensifies) and expands to lower latitudes. For severe storms, as in the case of March 13-14, 1989, the extent of the nightside aurora was observed below 40° magnetic latitude [*Vallance Jones*, 1992]. The observed peak polar cap potential drops associated with such a severe storm have been reported to exceed 300 kV [*Rich and Denig*, 1992]. This is quite large considering that the minimum or quiet time polar cap potential drop is approximately 35 kV [*Reiff et al.*, 1981].

The large values of potential that are observed during severe storms contradict an earlier report of *Weimer et al.* [1990b] which states that the saturation of the $AE(12)$ index during large geomagnetic activity is the result of a saturation in the polar cap potential drop. While *Rich and Denig* [1992] also report a saturation of the $AE(12)$ index, they found no evidence of the potential saturating. Instead, they found that the cross-polar cap potential increased as the width and the extent of the auroral zone increased. There are those [*Gonzales et al.*, 1994; *Feldstein*, 1992; *Tsurutani et al.*, 1985] who have suggested that the apparent saturation or even the decrease in $AE(12)$ for intense storms could be due to the fact that during such severe storms the auroral oval moves to considerably lower latitudes and the normal $AE(12)$ stations do not correctly monitor the storm's progression.

Although severe storms are by no means typical occurrences, there is a strong need for further investigation of these extreme cases. Severe storms deposit a significant amount of energy (in the form of both Joule heating and particle precipitation) into the Earth's auroral ionospheres. This can have far reaching effects on events such as thermospheric winds and atmospheric expansion and perhaps other, as yet unknown, consequences.

In this paper, we will use a data inversion model (AMIE; Assimilative Mapping of Ionospheric Electrodynamics) to calculate global electrodynamic parameters for a severe storm event. In addition, we will compare two of these parameters, the integrated Joule heating rate and the total polar cap potential drop, to both the $AE(12)$ index and the AE_{AMIE} index, an AMIE-modeled AE index created specifically for severe storms.

AMIE

The Assimilative Mapping of Ionospheric Electrodynamics (AMIE) data inversion model is detailed by *Kamide et al.* [1981], *Richmond and Kamide* [1988], and *Richmond* [1992]. Modifications upgrading the model are described by *Knipp et al.* [1993]. Essentially, AMIE employs a data inversion technique for mapping the high-latitude ionospheric electric field and currents using a combination of observed data from ground-based and satellite-based instruments. It also takes into account information on the interrelations of electrodynamic quantities and probable values of some electrodynamic features, such as average patterns, expected variability, and spatial correlation distances of electric fields. AMIE employs a grid spacing of every $1\frac{2}{3}°$ magnetic latitude and every 40 minutes magnetic local time (10° magnetic longitude). AMIE combines all of this information to come up with an optimized estimate of the electrodynamic features we desire, along with an indication of the accuracy of this estimate [*Richmond and Kamide*, 1988]. Uncertainty in the estimated electric field is calculated at every grid point. For this study, the uncertainties in some locations are high due to both

the sparse data coverage over a small portion of the northern hemisphere and the limited ability of the magnetometer data to help determine the convection during the darkness of November, when the conductivity is low.

For this study, we use the *Fuller-Rowell and Evans* [1987] model to calculate the initial conductance. It is derived from 6 years of particle precipitation data from the National Oceanic and Atmospheric Administration (NOAA) satellites and parameterized by the 10-level hemispheric power index. Error estimates for the calculated conductance are of the order of a factor of 2. For the initial estimates of electric potential, we use the model of *Foster et al.* [1986]. This model was derived from 7 years of plasma drift observations by the Millstone Hill radar facility. It is also parameterized by the hemispheric power index, but the information received from this model is used only as a priori information. The initial electric potential pattern produced from this model has little influence on the final mapped results.

There are some considerations for the errors that are inherent in the AMIE procedure. As with all inversion models, good coverage of data is essential for reliable results. Also, the dynamo effects of thermospheric winds which are usually unimportant at auroral latitudes are ignored along with the effects of the magnetospheric ring currents which could have an important influence at lower latitudes if not removed from the data. For the sake of simplicity, AMIE assumes that all currents above the ionosphere are strictly radial; that is, magnetic variations are associated only with the toroidal component of the height integrated ionospheric current. Also, estimates of currents within the Earth are calculated by using a perfectly conducting layer at depth 250 km, with a perfect insulator overtop. Just these last two assumptions alone could induce errors of the order of 10%.

For this study, we use four data sets as primary inputs into AMIE: ground magnetometer data, satellite electron precipitation data, satellite ion drift data, and ion drift velocities obtained from radar measurements. The 74 ground magnetometer stations (i.e., the Greenland Chain, the Alaskan Chain, the Canadian Auroral Network for the OPEN Program Unified Study (CANOPUS), the British Sub-Auroral Magnetometer Network (SAMNET), etc.) that were used for this 2-day period are listed in Table 1. AMIE works in the magnetic apex coordinate system [*VanZandt et al.*, 1972], where the X component points in the direction of the magnetic north pole. The declination is the angle between geographic north and local magnetic north, and Paleomagnetic Stability Index (PSI) is the angle between geographic north and magnetic apex north.

The magnetic variations needed as input for AMIE are the difference between the disturbed day values and the quiet day mean. The quiet day used for all of the stations was November 7, 1991. Also, during the preparation of the data for input into AMIE, the *Dst* effect is removed from the magnetic X (northward) component of all the stations. The cross-track component of the ion drift was measured by the Defense Meteorological Satellite Program (DMSP) Flight 8 (F8), Flight 9 (F9), and Flight 10 (F10) satellites, whereas the downward energy flux and mean energy of precipitating electrons, used in estimating auroral conductivities, were measured by the DMSP F8 and F9 satellites, the NOAA 12 satellite, and the Medium Energy Particle Spectrometer (MEPS) instrument on the Upper Atmospheric Research Satellite (UARS). The plasma drift radar data come from the Goose Bay HF radar facility.

We have undertaken the modification of AMIE to make it more suitable to the analysis of storms. AMIE was originally designed for the investigation of minor to moderate substorm activity levels. Initially, AMIE weighted the input data according to magnetic latitude with a boundary set so that the data measured below 50° magnetic latitude were considered less important for the auroral region. But, in the case of severe storms, the auroral zone can extend lower than this imposed boundary. Therefore AMIE's boundary was extended to 40° magnetic latitude so that the lower latitude data are now weighted heavier in the calculations and are included in the graphical output.

Polar Cap Potential Models

The potential drop across the polar cap is one of the most basic characteristics of high-latitude electrodynamics. It represents, in large part, the east-west interplanetary electric field that is mapped onto the ionosphere. It is often used in comparing different electrodynamic states since it is easier to compare polar cap potential values than trying to compare the widely differing electric potential patterns due to changing fields and currents in the polar cap during a storm.

There are many different ways to calculate the polar cap potential drop. Direct electric field measurements using incoherent scatter radar have been used to estimate the polar cap potential drop, but since the radar's field of view is small (in global terms), this type of measurement does not give an instantaneous measure of the global potentials. Calculating the potential from solar wind parameters using magnetic reconnection theories has proven to be useful [*Gonzales and Mozer*, 1974], along with integrating the measured electric field along the orbits of polar orbiting satellites [*Reiff et al.*, 1981; *Wygant et al.*, 1983; *Weimer et al.*, 1990b]. However, this method cannot ensure that the satellite trajectory cuts across the entire potential drop; rather, it is more likely to measure only a portion of the total potential. Another method, using empirical models such as IZMEM (Institute of Terrestrial Magnetism, Ionosphere and Radiowave Propagation (IZMIRAN) electrodynamic model, which employs a linear regressional analysis technique [*Papitashvili et al.*, 1994], can be implemented as long as the IMF data needed as input are available. Or one could use the data inversion model, AMIE.

Table 1. Magnetometer Stations Used in This Study

Station Name	Magnetic Apex Latitude	Magnetic Apex Longitude	Declination	PSI
Thule	85.62	34.76	-68.79	-38.49
Savissivik	83.88	36.81	-62.58	-36.24
Nord	80.91	106.59	-28.78	-47.11
Mould Bay	80.89	-89.11	53.53	45.07
Cambridge Bay	77.49	-53.32	23.57	26.09
Umanaq	77.18	44.41	-45.58	-30.12
Danmarkshavn	77.33	87.84	-26.68	-33.23
Sachs Harbour	76.33	-84.57	42.83	35.79
Godhavn	76.11	40.73	-44.36	-28.27
MAGIC (GISP)	75.69	67.21	-34.37	-30.37
Daneborg	75.23	81.16	-26.18	-29.15
Attu	74.89	39.23	-42.57	-26.98
Baker Lake	74.33	-34.14	1.29	13.85
Sondre Stromfjord	73.51	41.91	-40.10	-26.56
Contwoyto Lake	73.39	-59.23	-11.69	25.87
Rankin Inlet	73.26	-26.72	-6.38	9.04
Sukkertoppen	72.39	37.88	-39.02	-25.13
Scoresbysund	71.86	73.79	-25.21	-24.25
Inuvik	71.22	-87.58	35.66	30.30
Barrow	69.88	-110.37	25.20	25.66
Ammassalik	69.65	54.81	-31.72	-24.64
Yellowknife	69.65	-60.97	27.31	24.28
Fort Churchill	69.29	-28.95	0.71	10.00
Frederikshaab	68.44	39.49	-33.97	-23.53
Arctic Village	68.48	-99.15	29.66	26.99
Back	68.29	-28.86	0.88	9.87
Fort Smith	67.84	-56.09	23.08	21.86
Fort Simpson	67.60	-68.82	29.36	25.16
Rabbit Lake	67.57	-43.63	13.74	17.06
Narsarsuaq	66.75	43.79	-31.57	-23.19
Poste-de-la-Baleine	66.24	-2.19	-19.25	-6.41
Fort Yukon	67.18	-96.63	29.28	26.23
Gillam	66.96	-29.32	2.04	10.01
Dawson	65.95	-89.09	29.29	25.97
Tixie Bay	65.79	-163.04	-13.86	-2.23
Leirvogur	65.34	67.91	-21.11	-19.49
College	65.00	-97.35	27.00	24.44
Fort McMurray	64.72	-53.42	19.69	19.80
Island Lake	64.52	-28.89	2.73	9.66
Sodankyla	63.97	108.05	6.83	-7.39
Meanook	62.29	-55.28	20.43	19.51
Talkeetna	61.97	-97.45	24.57	22.43
Oulu	61.72	106.04	6.02	-6.37
Nordli	61.60	95.65	-0.43	-7.50
Faroes	60.94	78.25	-11.31	-13.30
Anchorage	60.95	-96.60	24.17	21.99
Pinawa	60.80	-30.39	4.84	10.26
Glenlea	60.08	-31.84	6.33	10.90
Sitka	59.86	-80.98	25.99	22.40
Lerwick	58.17	81.76	-7.47	-10.46
Nurmijarvi	56.90	102.77	4.73	-4.14
Lovo	55.93	96.61	1.79	-5.12
Newport	55.13	-57.47	18.67	17.71
Glenmore	55.10	78.33	-7.92	-10.02
St Johns	54.48	31.04	-23.42	-20.51
Victoria	54.01	-64.66	20.37	18.41

Table 1. (continued)

Station Name	Magnetic Apex Latitude	Magnetic Apex Longitude	Declination	PSI
Eskdalemuir	52.94	77.92	-7.18	-9.19
Brorfelde	52.14	90.05	-0.66	-5.01
York	51.14	79.11	-5.85	-7.96
Fredericksburg	49.74	-3.13	-8.82	-4.29
Boulder	49.24	-41.08	11.17	13.19
Hartland	48.10	75.34	-6.72	-8.09
Chambon-la-Foret	43.89	79.91	-3.45	-4.81
Fresno	43.22	-56.90	15.02	14.09
Bay St. Louis	41.69	-20.14	1.95	6.99
Tucson	40.01	-46.04	11.70	12.58
Del Rio	39.48	-34.38	8.03	11.26
Memambetsu	36.66	-145.15	-8.07	-1.75
San Juan	29.07	9.49	-10.70	-14.11
Kakioka	28.83	-148.75	-6.28	-2.18
Kanoya	24.22	-157.60	-5.28	-2.96
Honolulu	21.66	-90.71	10.99	8.71
Lunping	17.89	-167.38	-3.01	-1.78
Guam Island	5.55	-144.57	1.81	1.86

PSI is the Paleomagnetic Stability Index.

Of particular interest in severe storm investigations is to use a global electrodynamic model, like AMIE, to estimate not only the electric potential but also Joule heating and auroral inputs. These global values are necessary inputs for models of the thermosphere such as the TIGCM (Thermosphere/Ionosphere General Circulation Model) described by *Roble et al.* [1988].

Results

Figures 2a and 2b show the temporal variations for two of the electrodynamic quantities calculated by AMIE during the 2-day interval November 8-9, 1991: the integrated Joule heating poleward of 40° magnetic latitude, H_J, and the total potential drop across the polar cap, Φ.

Joule Heating

A fraction of the kinetic energy flux of the solar wind, impinging on the dayside magnetopause, is extracted by several different mechanisms and enters the Earth's magnetosphere. Much of the energy is ultimately dissipated in the polar ionospheres. Some of the energy is directly transferred to the high-latitude ionospheres

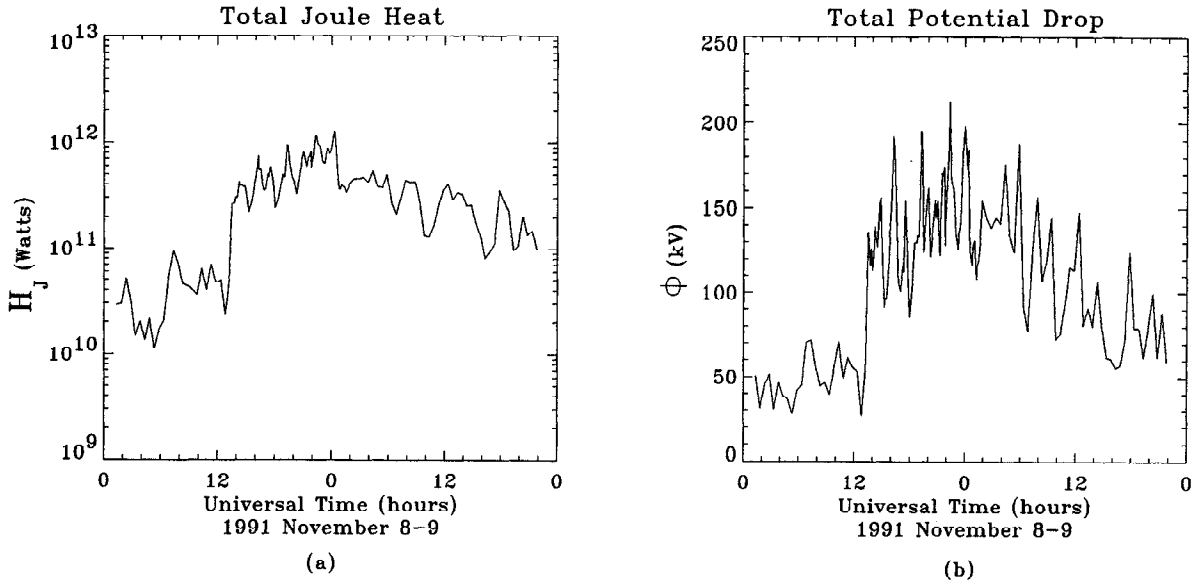

Figure 2. The temporal variations for two of the Assimilative Mapping of Ionospheric Electrodynamics (AMIE) calculated global parameters: (a) the integrated Joule heating poleward of 40° magnetic latitude, H_J, and (b) the total polar cap potential drop, Φ.

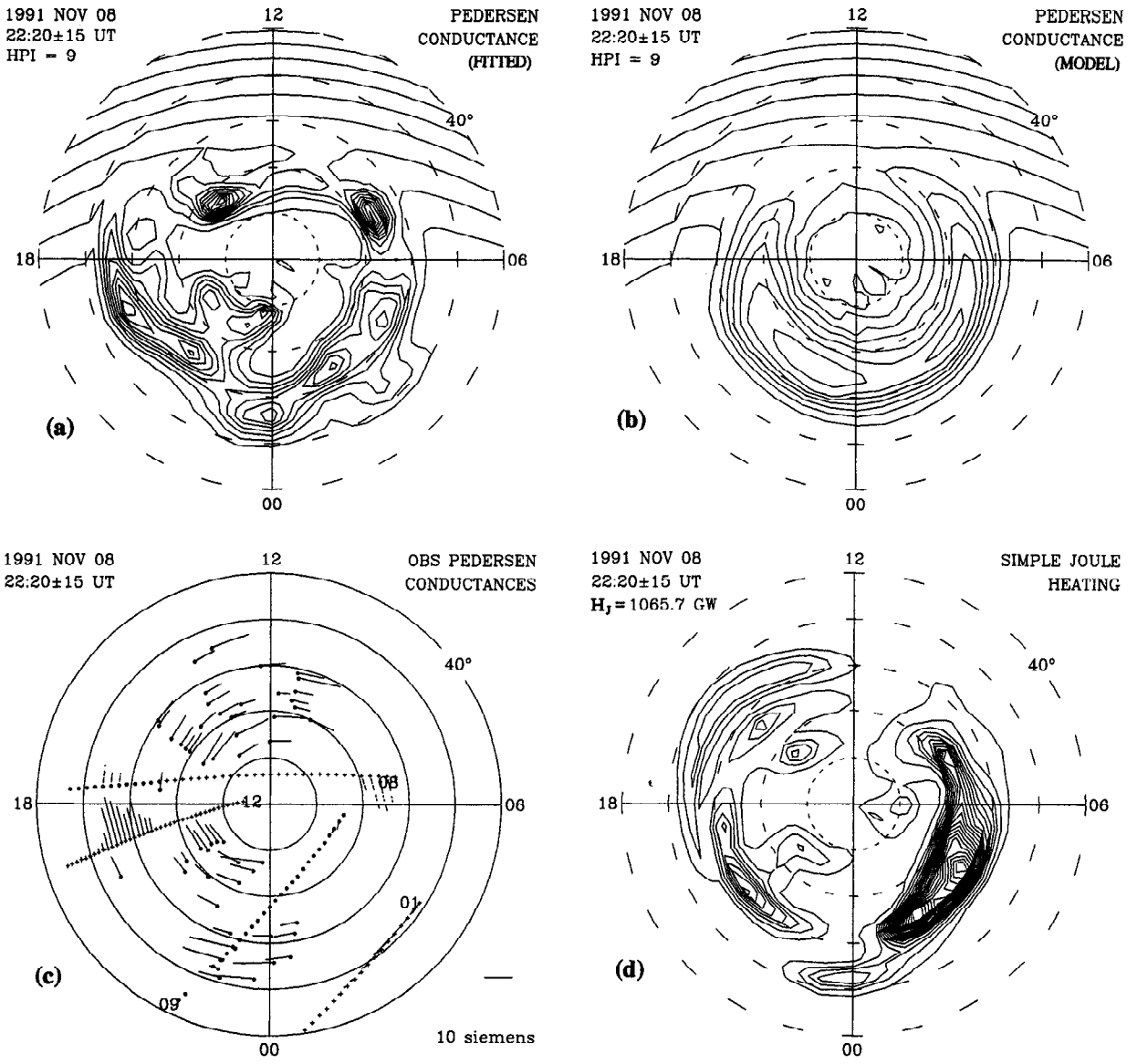

Figure 3. (a) The modified Pedersen conductance which takes into account actual observations available on November 8, 1991, 2220 UT. (b) The model of the Pedersen conductance for a hemispheric power index (HPI) of 9, after *Fuller-Rowell and Evans* [1987], with an additional solar-ultraviolet component appropriate to November 8, 1991, 2220 UT. In Figures 3a and 3b the contour intervals are 2 Siemens (S). (c) The observed Pedersen conductances indicated by the magnitudes of the displayed vectors from both satellite passes and magnetometer data. The dashed lines indicate data from the southern hemisphere, used here by assuming conjugacy. (d) A contour plot of the Joule heating near the peak of the storm. Contour intervals are 10 mW/m^2 and H_J is the total Joule heating rate poleward of 40° magnetic latitude. Coordinates are magnetic latitude and magnetic local time (MLT).

through field-aligned currents which are driven by the solar wind MHD dynamo. Energy that has been stored in the magnetotail is another source. A study by *Lu et al.* [1995] suggests that over 90% of the electromagnetic energy dissipated from the magnetosphere to the ionosphere is converted into Joule heating. The energy is transferred to the auroral ionosphere through particle precipitation and field-aligned currents and dissipated in the form of Joule and particle heating during substorms [*Kamide and Baumjohann*, 1993]. Joule heating can make a significant energy contribution to the upper atmosphere at high latitudes and can even be the dominant heat source above 120 km during large magnetic storms. This heating of the upper atmosphere can affect thermospheric winds and causes the expansion of the upper atmosphere to change the orbits of near-Earth satellites due to increasing drag. In addition, the amount of energy deposited to the atmosphere during severe storms causes vertical motions in the thermosphere that redistribute species and thus change the composition in that region. Joule heating may also have other, as yet unknown, consequences.

The AMIE-calculated Joule heating assumes a zero neutral wind and uses the Pedersen conductance times

the square of the electric field. This calculation does not take into consideration any changes caused by the uncertainties in the electric field. The total Joule heating for November 8-9, 1991, given in Figure 2a has a range of approximately 20 GW ($\sim 10^{10}$ W) during the quiet period occurring just before the storm to just over 1000 GW ($\sim 10^{12}$ W) at the peak of the storm. Typically, for moderately disturbed periods the maximum total Joule heating that is observed is around 600 GW [*Richmond et al.*, 1990].

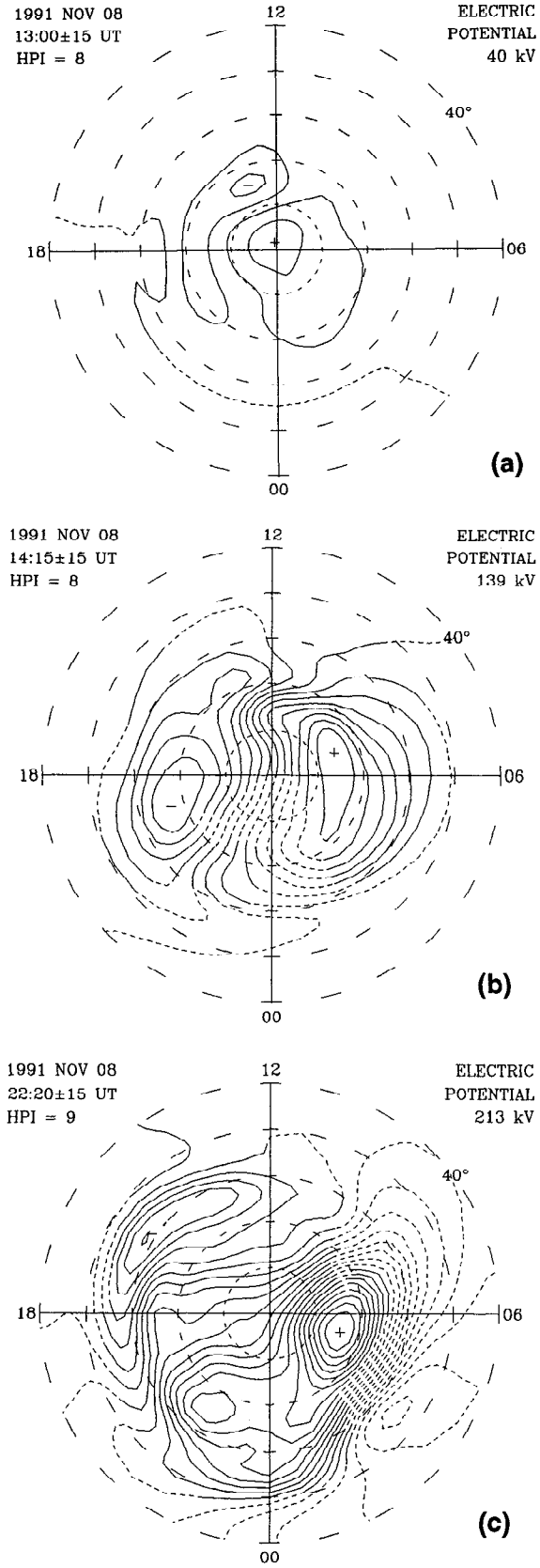

Figure 3a shows the contours of the fitted Pedersen conductance for 2220 UT near the peak of the storm, while Figure 3b shows the modeled Pedersen conductances for the 9th level of the hemispheric power index [*Fuller-Rowell and Evans*, 1987]. Figure 3a is obtained by modifying this modeled conductance pattern based upon observations shown in Figure 3c. The Pedersen observations include the estimates using *Robinson et al.* [1987] formula relating measurements of the auroral electron energy flux and mean electron energy to the Hall and Pedersen conductance. DMSP and UARS measure electron precipitation which is converted to conductance using the techniques described by *Rich et al.* [1987]. Figure 3c shows the observed Pedersen conductances derived from satellite particle data and from ground magnetometer data. The conductances are shown as the magnitudes of the displayed vectors. The numbers positioned near a satellite pass indicate from which satellite the data were taken from: 01 is the UARS satellite, 12 is the NOAA 12 satellite, 08 is the DMSP F08 satellite, and 09 is the DMSP F09 satellite. The dashed lines which are used for the DMSP F08 satellite indicate that the data were measured in the southern hemisphere. Conjugacy is assumed for particle precipitation, so observations from both hemispheres are used. Additional rough estimates of the conductance are provided by the ground magnetic perturbations under the electrojets from stations between 50° and 78° magnetic latitude using formulas similar to the ones given by *Ahn et al.* [1983b].

Comparing Figures 3a, 3b and 3c, the differences between the model and fitted conductances are located only where we have observed data; otherwise, there is no significant change to the original model given by *Fuller-Rowell and Evans* [1987]. The changes caused by satellite data are fairly accurate, but the changes that have been influenced by mainly magnetometer data are only rough estimates, in which the strength of the conductance is directly proportional to the strength of the X component. Also, the magnetometers register data related to both auroral and solar-ultraviolet conductances, while the satellites measure data only re-

Figure 4. The AMIE calculated potential distributions for (a) 1300 UT and (b) 1415 UT November 8. Figures 4a and 4b represent the time just before the onset of the storm and the time right after the start of the storm, respectively. (c) The maximum potential drop for the 2-day period occurs at 2220 UT. The contour interval for all of the potential plots is 10 kV, and contours are dashed where the estimated uncertainty in the large-scale electric field exceeds 50%. The potential high and low are indicated by a plus and minus, respectively. The total potential drop is written at the upper right of each diagram, and the hemispheric power index (HPI) is also indicated.

lated to auroral conductances. For example, in Figure 3c, we see that the NOAA 12 satellite defines the dusk auroral conductance very well, approximately 19 magnetic local time (MLT) and between 60° and 50° magnetic latitude. From this, we see that the peak value of the conductance in the dusk region is located at low latitudes, around 55°. However, the increase in conductance located around 15 MLT and roughly between 70° and 78° latitude could, in fact, be more likely due to other sources such as distant field-aligned currents which the ground magnetometers in that region would register.

In Figure 3d, the contours of the Joule heating are shown to be vary large near the predawn region. Comparing this to the results of the conductance in that region (Figure 3a), the conductance is not as high as one would expect. However, the potential distribution in Figure 4c shows that in this region there is a very large gradient of electric potential which is the reason for the large magnitude of Joule heating.

The contours of the Joule heating also show the regions of major heat production near the peak of the storm. The position of these regions can be used as a rough estimate for the position of the auroral electrojets. Figure 3d shows that the regions of major heat production extend to 65° magnetic latitude, indicating that the auroral electrojets now extend to 65° also. Our analysis indicate, that the auroral electrojets are around 65° from approximately 1900 UT November 8 until around 0200 UT November 9.

As comparison, for example, the March 22, 1979, Coordinated Data Analysis Workshop (CDAW) 6 substorm interval may be considered a minor storm with *Dst* developing to nearly −80 nT [*Tsurutani et al.*, 1985]. Using the Kamide Richmond Matsushita (KRM) [*Kamide et al.*, 1981] data inversion scheme for this interval, *Reiff et al.* [1985] found the polar cap potential drop which obtained a magnitude of 240 kV for short intervals. The total Joule heating found by *Kamide and Baumjohann* [1985] and *Kroehl and Kamide* [1985] reached magnitudes of 10^{12} W. For the November 8-9, 1991 storm, we obtain similar values for potential and Joule heating rate, but for a longer duration.

High rates of heat production $\mathbf{J} \cdot \mathbf{E}$ can result from regions where either $\mathbf{J}$ or $\mathbf{E}$ or both are large. Spatial separation of major heating sources suggests that the relative importance of ionospheric conductivity and electric field in carrying ionospheric currents may differ considerably over the electrojet regions. This has been observed with direct observations of the electric field and conductance during moderate activity conditions using the Chatanika Radar [*Vickery et al.*, 1982; *Kamide and Vickery*, 1983]. The relative spatial variability of the electric field and conductance is a fundamental problem yet to be measured for magnetic storms and particularly for major or severe storms.

Polar Cap Potential

The total potential drop is calculated as the difference between the minimum and maximum electric potentials found poleward of 40° magnetic latitude. Results for the total potential during the 2-day period indicate a range of values from a minimum of 40 kV at 1300 UT November 8 just before the onset of the storm to a maximum of 213 kV calculated for the peak storm activity at 2220 UT November 8. Figures 4a and 4b show the calculated potential distributions for 1300 UT November 8 and 1415 UT November 8, which represent the time right after the start of the storm. The maximum potential drop occurring at 2220 UT November 8 is shown in Figure 4c.

While the total potential drop is a fundamental characteristic of high-latitude electrodynamics, the electric potential pattern itself can be very useful. During the November 8-9, 1991 storm, direct measurements of the IMF are unavailable, but, in Figure 4, a distinct two-cell electric potential pattern showing antisunward convection across the pole indicates, according to reconnection theories, that the Z component of the IMF was southward (negative) throughout the storm.

AMIE Modeled AE

The standard $AE(12)$ index is calculated from the N-S components of the magnetic field perturbations at 12 magnetometer stations ranging from 60° to 71° magnetic latitude and placed around the polar cap at fairly even intervals in magnetic longitude. It was originally meant to estimate the magnitude of the auroral electrojets, the eastward and westward currents flowing in the auroral ionosphere. The $AE(12)$ index is reasonably accurate for moderately active intervals [*Akasofu et al.*, 1983], when the auroral electrojets are in position above these 12 stations, but during either periods of quiet or severely disturbed intervals, the position of the auroral electrojets has moved either poleward or equatorward from the position of the 12 stations. For example, during a severe storm, the auroral electrojets may still be increasing in strength, but the $AE(12)$ stations that are now poleward of the currents will not record the full magnitude. In order to accurately measure the magnitude of the auroral electrojets, especially during severe storms, we would need to be able to "track" the currents

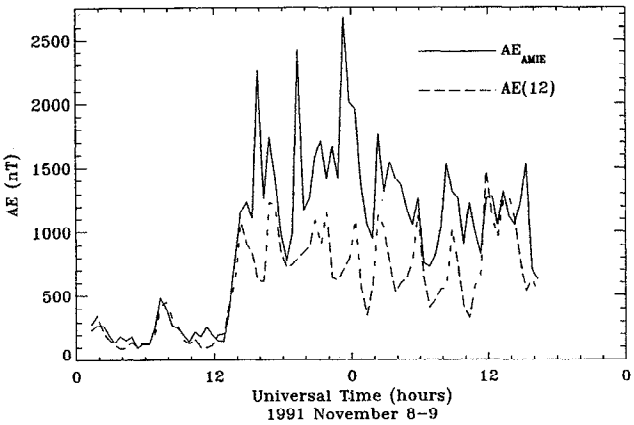

Figure 5. The time variation of the AE_{AMIE} index and the $AE(12)$ index during the November 8-9, 1991, time period.

Table 2. Results of the Total Joule Heating, H_J, Versus AE

Paper	Linear Equation	Correlation Coefficient
Present study	$H_J = -20 + 0.28AE_{\mathrm{AMIE}}$	0.62
	$H_J = -49 + 0.54AE(12)$	0.62
Richmond et al. [1990]	$H_J = 1.8 + 0.21AE(12)$	0.88
Ahn et al. [1989]	$H_J = 0.33AE(12)$	0.90
Baumjohann and Kamide [1984]	$H_J = 0.32AE(12)$	0.74
	$H_J = 0.33AE(71)$	0.87
Ahn et al. [1983a]	$H_J = 0.23AE(12)$	...
	$H_J = 0.19AE(71)$	...

H_J is in gigawatts, and AE is in nanoteslas.

throughout the progression of the storm. If we had an array of stations evenly spaced in magnetic longitude and ranging in magnetic latitude from the position of the auroral electrojets during minimally active intervals to its position during severely disturbed intervals, then we would be able to effectively track the currents.

One of the advantages of the AMIE technique is that once the high-latitude ionospheric electric field and currents are found, it is then possible to predict the magnetic fluctuations occurring on the ground at any point poleward of 40° magnetic latitude. We have used this feature to calculate the AE_{AMIE} index during the November 1991 storm when the auroral electrojets moved to latitudes below the standard $AE(12)$ stations. The AE_{AMIE} index is calculated from the N-S components of the AMIE modeled magnetic field perturbations in the range of 72° to 42° magnetic latitude by 2° increments and from 0° to 360° magnetic longitude by 15° increments. This distribution gives us good coverage during many different strengths of magnetic activity so that we are sure to find the true magnitude of the auroral electrojets.

For this study, the standard $AE(12)$ index was unavailable; however, data from most of the magnetometers used to calculate the $AE(12)$ index were available. Thus a nearly standard $AE(12)$ index was calculated for November 8-9, 1991, by replacing four unavailable stations with available stations located at approximately the same magnetic latitude and as close to the same magnetic longitude as was possible (e.g., Cape Wellen (61.79°, 237.10°) replaced by Talkeetna (61.97°, 262.55°)).

Figure 5 shows the variation in time of the nearly standard $AE(12)$ index and the AE_{AMIE} index. They have a high correlation of 0.97 for the period just before the onset of the storm, but, as the storm develops, the values begin to vary widely from each other. They have a correlation of only 0.73 for the total 2-day interval, and, on average, the value of AE_{AMIE} was 1.569 larger than the $AE(12)$.

We feel that the AE_{AMIE} index with its maximum value of 2669 nT is roughly what one would see if there really were stations located every 2° in latitude and every 15° in longitude. In order to show that AMIE does a good job of modeling these magnetic perturbations at ground level, we calculate from the modeled data a "simulated" $AE(12)$ index by looking at just a single ring of stations at 66° magnetic latitude to represent the standard stations. In doing so, we get a very good correlation of 0.93 between the two indices with a maximum "simulated" $AE(12)$ of 1620 nT which roughly matches that of the $AE(12)$ index's maximum of 1470 nT.

Joule Heating Versus AE

Previous studies on the relationship of the total Joule heating versus the AE index [*Richmond et al.*, 1990; *Ahn et al.*, 1989; *Baumjohann and Kamide*, 1984; *Ahn et al.*, 1983a] have found a significant linearity between the two values. The resulting equations, given in Table 2, are in agreement with each other, and any small differences between them may be due to the different methods used in estimating Joule heating. In addition, seasonal variations can have a direct effect on the ionospheric conductivities, which in turn affects Joule heating. There was a similar result by *Lu et al.* [1995], but the relationship, $P = -26 + 0.33AE(12)$, was given for P, the hemispheric energy dissipation, and the $AE(12)$ index. The hemispheric energy dissipation is mainly due to Joule heating, but it also includes the mechanical power supplied due to the acceleration of the wind. Another study [*Vickery et al.*, 1982] found no striking relationship between Joule heating and AE, but their results could be due to the fact that for a moderate storm period, they used an AE index calculated from only five magnetometer stations. However, all of these previous equations were based on the results for only minor to moderate activity levels; not one included highly disturbed activity levels.

Going on the assumption that there is a linear relationship between total Joule heating and the AE index, Figure 6 shows the calculated AMIE total Joule heating, H_J, in gigawatts, versus the $AE(12)$ index, in nanoteslas. A linear fit to the data produced the equation

$$H_J = -49 + 0.54AE(12) \quad (1)$$

with a correlation coefficient of 0.62.

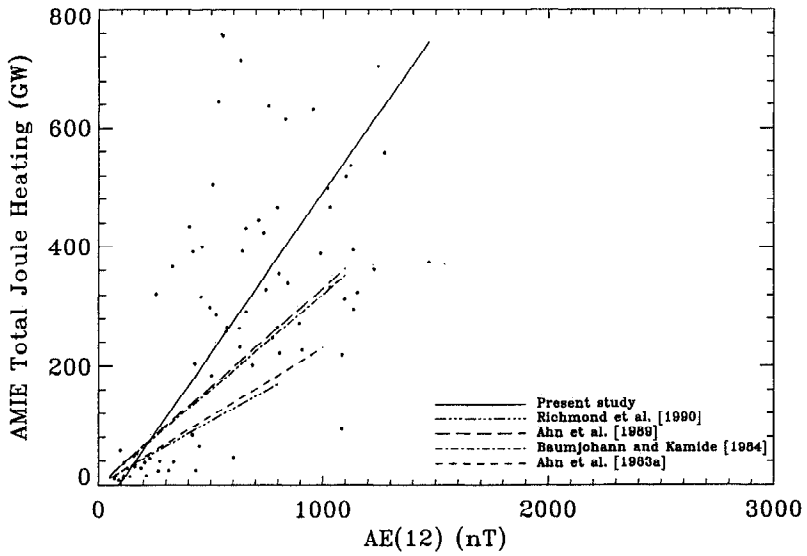

Figure 6. The relationship between the AMIE calculated total Joule heating, H_J, and the nearly standard $AE(12)$ index. The dashed and dot-dashed lines represent the total Joule heating - $AE(12)$ index relationships obtained by *Richmond et al.* [1990], *Ahn et al.* [1989], *Baumjohann and Kamide* [1984], and *Ahn et al.* [1983a].

Figure 7 shows the calculated AMIE total Joule heating, H_J, in gigawatts, versus the AE_{AMIE} index, in nanoteslas. A linear fit to the data produced the equation

$$H_J = -20 + 0.28 AE_{\mathrm{AMIE}} \qquad (2)$$

with a correlation coefficient of 0.62.

We find that equation (1), which uses $AE(12)$, is not in good agreement with the equations from the previous studies. However, equation (2), which uses AE_{AMIE}, is similar to those equations given in Table 2. We suggest that the reason that equation (1) using $AE(12)$ is not similar to the previous studies is a consequence of the auroral electrojets moving away from the $AE(12)$ stations during the peak of the storm. This will result in high rates of Joule heating being paired with lower values of $AE(12)$ which would cause the slope of the equation to be steeper.

For our storm period, if we use only AE values below 1000 nT, we find that our equations do not noticeably change for either the $AE(12)$ index or the AE_{AMIE} index. However, the correlation coefficient for H_J versus $AE(12)$ increases to 0.73 while the correlation coefficient for H_J versus AE_{AMIE} increases to 0.87. Such

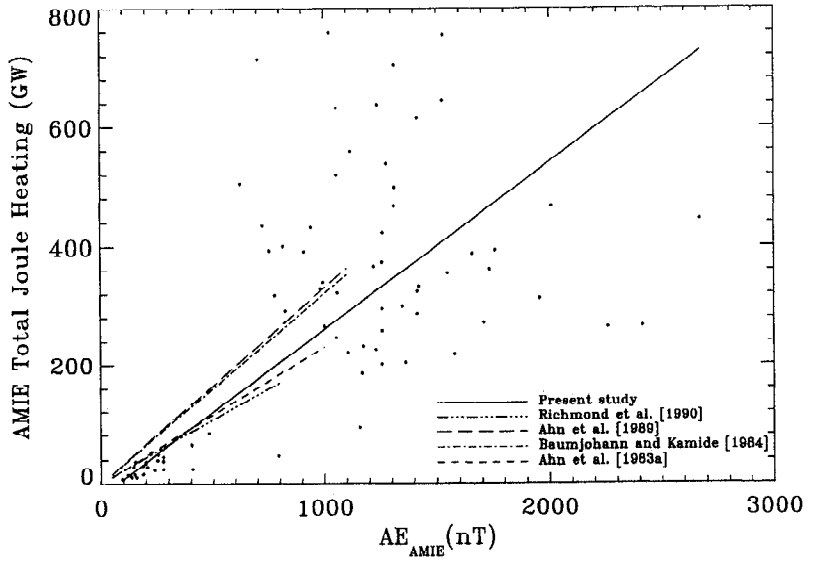

Figure 7. The relationship between the AMIE calculated total Joule heating, H_J, and the AE_{AMIE} index. The dashed and dot-dashed lines represent the total Joule heating - $AE(12)$ index relationships obtained by *Richmond et al.* [1990], *Ahn et al.* [1989], *Baumjohann and Kamide* [1984], and *Ahn et al.* [1983a].

Table 3. Results of the Total Polar Cap Potential, Φ, Versus AE

Paper	Linear Equation	Correlation Coefficient
Present study	$\Phi = 32 + 0.073 AE_{\mathrm{AMIE}}$	0.80
	$\Phi = 33 + 0.106 AE(12)$	0.65
Ahn et al. [1992]	$\Phi = 36 + 0.082 AE(12)$	0.80
Richmond et al. [1990]	$\Phi = 22 + 0.119 AE(12)$	0.88
Weimer et al. [1990a]	$\Phi = 26.8 + 0.152 AE(12)$ (winter)	...
	$\Phi = 19.2 + 0.116 AE(12)$ (summer)	...
Ahn et al. [1984]	$\Phi = 36 + 0.089 AE(12)$	0.83
Reiff et al. [1981]	$\Phi = 41 + 0.11 AE(12)$	0.71

Φ is in kilovolts, and AE is in nanoteslas.

a large increase in the correlation coefficient for the AE_{AMIE} results suggests that this is a better index than $AE(12)$ for moderate storm times as well.

In Figure 7, we see that there is significant amount of scatter associated with the data for the higher values of AE ($AE > 1000$ nT). The calculation of the Joule heating could be, in large part, responsible for this. As stated before, the conductance model is better suited to minor and moderate storm times. This alone could cause the Joule heating rates to become less accurate as the storm intensifies. Another possibility is that the scatter is a real feature of the relationship between Joule heating and AE during a severe magnetic storm.

Potential Versus AE

There have been previous results showing that for moderately active times the relationship between the $AE(12)$ index and the total polar cap potential, Φ, is approximately linear [*Reiff et al.*, 1981; *Ahn et al.*, 1984; *Richmond et al.*, 1990; *Weimer et al.*, 1990a]. The resulting linear equations, given in Table 3, are in agreement with each other. In a similar study using a more disturbed interval, *Weimer et al.* [1990b] suggested that the magnetosphere-ionosphere coupling is actually nonlinear and that the apparent saturation of the $AE(12)$ index is a natural consequence of a nonlinear system being driven beyond a certain limit. At one point, they suggest that the saturation could be due to the shift of the auroral electrojets' position but dismiss this explanation due to the fact that the electrojets remain poleward of 60° throughout the interval of study. However, even if the electrojets were poleward of 60° at all times, there is no guarantee that the position of the $AE(12)$ stations was in fact beneath the maximum value of the electrojets at a given time. A couple of degrees off and the value for the $AE(12)$ index could be underestimated by many nanoteslas. For our severe storm period, we know that the auroral electrojets were near 65° magnetic latitude during the peak of the storm. Therefore half of the $AE(12)$ stations were poleward of the auroral electrojets, giving AE values much lower than the actual value.

Figure 8 shows the calculated AMIE total polar cap potential drop, Φ, in kilovolts, versus the $AE(12)$ index, in nanoteslas. The relationship between the two can be approximated with the linear relationship

$$\Phi = 33 + 0.106 AE(12) \tag{3}$$

With a correlation coefficient of 0.65, this is not a good approximation for the relationship between the $AE(12)$ and severe storm potentials.

Figure 9 shows the calculated AMIE total polar cap potential drop, Φ, in kilovolts, versus the AE_{AMIE} index, in nanoteslas. The relationship between the two can be approximated with the linear relationship

$$\Phi = 32 + 0.073 AE_{\mathrm{AMIE}} \tag{4}$$

with a correlation coefficient of 0.80.

Equation (3) is very similar to other results found by using the $AE(12)$ index (Table 3). The correlation coefficient might have been higher if we hadn't included the points near the peak of the storm, but the equation itself wouldn't change. Equation (4) has a much better correlation coefficient, showing that this equation is a better approximation for the relationship between the severe storm potentials and the auroral electrojet strengths.

Weimer et al. [1990b] stated that polar cap potential saturates along with the $AE(12)$ index due to the nonlinear response of the polar cap potential to large magnetospheric potential imposed by enhanced reconnection on the dayside magnetopause. In order for this to be true, the maximum total polar cap potential drop for the November 1991 storm could not exceed the value of 188 kV, according to our results given in equation (3). But AMIE's results show that the potential reaches a value of 213 kV at 2220 UT on November 8. So then, if we input the maximum AE_{AMIE} value of 2669 nT into equation (4), we calculate a maximum polar cap potential as high as 227 kV. This is close to what AMIE calculated for the maximum potential. However, it should be noted that although the polar cap potential may not saturate at the values that we've seen so far, this does not mean that it won't saturate at a higher value.

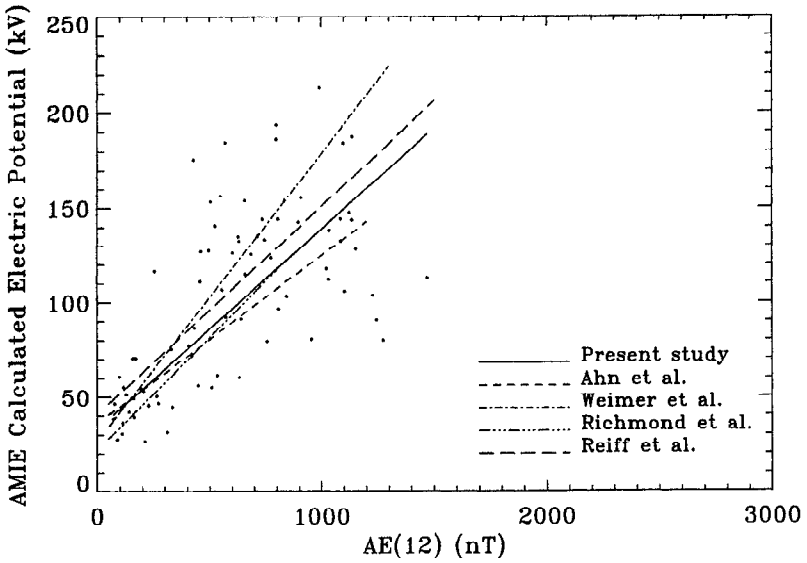

Figure 8. The relationship between the AMIE calculated polar cap potential, Φ, and the nearly standard $AE(12)$ index. The dashed and dot-dashed lines represent the polar cap potential - $AE(12)$ index relationships obtained by *Ahn et al.* [1984], *Weimer et al.* [1990a] (winter), *Richmond et al.* [1990], and *Reiff et al.* [1981].

Summary and Discussion

In this paper, we have used the data inversion model, AMIE, to calculate some of the global parameters which help to define the electrodynamic state of the ionosphere during the November 8-9, 1991 severe storm. In order to achieve this goal, a modification of the model extending its boundaries to include observed data poleward of 40° magnetic latitude was required. With this modification, we have made a reasonable first attempt of a global characterization of severe storms. However, for further severe storm studies, a future modification of AMIE would have to include a conductivity model better suited to disturbed activity levels.

The current conductivity model by *Fuller-Rowell and Evans* [1987] is an averaged model. Thus, for average activity levels, i.e., moderate or minor storms times, the model does a fairly good job, but the model does not include a sufficient number of severe storm times, and therefore it would tend to smooth any peaks and broaden the region of enhanced conductance. The effect of using this model as a starting point for severe storm conductances is uncertain. However, the conductance model does play an important role in calculating the

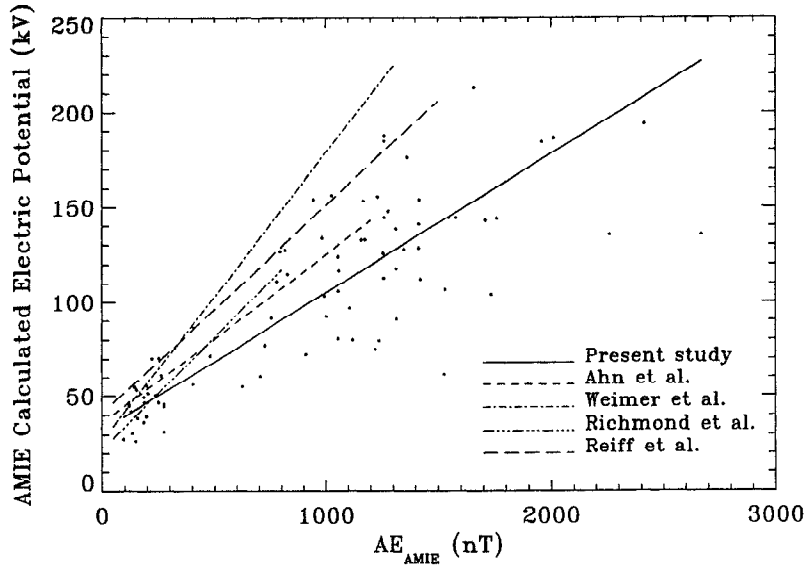

Figure 9. The relationship between the AMIE calculated polar cap potential, Φ, and the AE_{AMIE} index. The dashed and dot-dashed lines represent the polar cap potential - $AE(12)$ index relationships obtained by *Ahn et al.* [1984], *Weimer et al.* [1990a] (winter), *Richmond et al.* [1990], and *Reiff et al.* [1981].

integrated Joule heating rate. Thus using the present conductance model would definitely effect Joule heating rates, and due to the availability of satellite data, each time interval studied would be individually affected. If we have a good coverage of satellite passes for a particular time interval, then we would have better estimates of conductance and therefore better estimates of the Joule heating rate. But, if we had poor satellite coverage, then the estimates of conductance and Joule heating would be poor for that time interval. Consequently, the lack of a "storm-time" conductance model may be the reason that the integrated Joule heating rate for the November 1991 severe storm is approximately equal to that found during the March 1979 moderate substorm. Therefore, before further storm investigations can be realized, the development of a conductance model better suited to storm-time activity levels should be undertaken.

It should be noted, however, that while the magnitudes of the total Joule heating are comparable for the November 1991 severe storm and the March 1979 moderate substorm, the amount of time that this value was sustained is quite different. The substorm had values of Joule heating which exceeded 100 GW (10^{11} W) for a period of 7 hours while the severe storm exceeded that same value for almost an entire day ($\sim$ 22 hours). From this, it is clear that the severe storm had a more significant impact on the upper atmosphere than that of the moderate substorm.

Results obtained from the total Joule heating versus the $AE(12)$ index do not agree with those found in previous reports (Table 2). However, the equation obtained from the total Joule heating versus the AE_{AMIE} index closely resembles the other equations that were found during much less disturbed times using the $AE(12)$ index. Our results using the $AE(12)$ index appear to saturate at a level around 1300 nT. However, this saturation is associated with the location of the stations used in the calculation of the $AE(12)$ index and not a physical result. Previous studies which used the $AE(12)$ index did not show signs of saturation because they did not include severe storm times in their calculations and, in general, do not have values of AE greater than 1000 nT. The low correlation coefficients associated with our results can be attributed to the values of total Joule heating during the more disturbed intervals of the storm. The calculation of Joule heating is uncertain for the more severe time intervals which include few satellite passes. If we were to just take the data associated with values of AE below 1000 nT, we find that our equations do not noticeably change for either the $AE(12)$ index or the AE_{AMIE} index. However, the correlation coefficient for the $AE(12)$ index only increases to 0.73 while the correlation coefficient for the AE_{AMIE} index increases to 0.87. Such a large increase in the correlation coefficient for the AE_{AMIE} results suggests that this is a better index than $AE(12)$ for moderate storm times as well.

An apparent saturation of the $AE(12)$ index can also be seen in our comparison of the polar cap potential with the $AE(12)$ index, but this is not the case when using the AE_{AMIE} index. The comparison between the polar cap potential and the AE_{AMIE} index yields an approximate linear relationship with a correlation coefficient of 0.80. From our results, we find that the magnitude of the auroral electrojets and the polar cap potential drop do not show signs of saturation at the activity levels that were present during the November 8-9, 1991 severe storm.

Acknowledgments. MAGIC magnetometer data and partial support for this work at the University of Michigan have been provided by NSF grant ATM-9204520. Partial support for this work was provided by NASA contract NA55-27753 at the Southwest Research Institute. Support at the High Altitude Observatory of the National Center for Atmospheric Research was provided by NASA Work Order W-17,385. This study made use of the CEDAR (Coupling, Energetics and Dynamics of the Atmospheric Regions) Data Base located at the National Center for Atmospheric Research (NCAR), which is supported by the National Science Foundation. Seventy-four ground magnetic observatories contributed to this study. Forty-nine of these were processed through the World Data Center A in Boulder. We are indebted to L. Morris of that facility. We thank Eigil Friis-Christensen of the Danish Meteorological Institute in Denmark for the Greenland chain magnetometer data. We thank Terry Hughes for the CANOPUS magnetometer data. The CANOPUS instrument array was constructed and is maintained and operated by the Canadian Space Agency for the Canadian scientific community. We thank Tim Yeoman and Dave Milling of the University of Leicester in England for the SAMNET magnetometer data. We thank Mike Ruohoniemi for the Goose Bay HF radar data. The Goose Bay HF radar is operated by the Applied Physics Laboratory of The Johns Hopkins University with support from the National Science Foundation. We thank Bill Denig at the Phillips Laboratory for the DMSP electron precipitation data. We thank Fred Rich at the Phillips Laboratory for the DMSP ion drift data. We thank the Space Environment Lab (SEL), especially Dave Evans, for the NOAA 12 data. We thank Rudy Frahm at the Southwest Research Institute (SWRI) for the Medium Energy Particle Spectrometer (MEPS) data obtained from the Particle Environment Monitor (PEM) aboard the Upper Atmospheric Research Satellite (UARS). We thank Dave Chenette at Lockheed for the Atmosphere X ray Imaging Spectrometer (AXIS) data obtained from the Particle Environment Monitor (PEM) aboard the Upper Atmospheric Research Satellite (UARS).

The Editor thanks W. F. Denig and R. J. Pellinen for their assistance in evaluating this paper.

References

Ahn, B. H., H. W. Kroehl, Y. Kamide, and D. J. Gorney, Estimation of ionospheric electrodynamic parameters using ionospheric conductance deduced from Bremsstrahlung x ray image data, *J. Geophys. Res., 94*, 2565, 1989.

Ahn, B. H., S.-I. Akasofu, and Y. Kamide, The Joule heat production rate and the particle energy injection rate as a function of the geomagnetic indices AE and AL, *J. Geophys. Res., 88*, 6275, 1983a.

Ahn, B. H., R. M. Robinson, Y. Kamide, and S.-I. Akasofu, Electric conductivities, electric fields and auroral energy injection rates in the auroral ionosphere and their empirical relations to the horizontal magnetic disturbances, *Planet. Space Sci., 31*, 641, 1983b.

Ahn, B. H., S.-I. Akasofu, Y. Kamide, and J. H. King, Cross-polar cap potential drop and the energy coupling function, *J. Geophys. Res.*, *89*, 11,028, 1984.

Ahn, B. H., Y. Kamide, H. W. Kroehl, and D. J. Gorney, Cross-polar cap potential difference, auroral electrojet indices, and solar wind parameters, *J. Geophys. Res.*, *97*, 1345, 1992.

Akasofu, S.-I., B. H. Ahn, Y. Kamide, and J. H. Allen, A note on the accuracy of the auroral electrojet indices, *J. Geophys. Res.*, *88*, 5769, 1983.

Baumjohann, W., and Y. Kamide, Hemispherical Joule heating and the AE indices, *J. Geophys. Res.*, *89*, 383, 1984.

Feldstein, Y. I., Modeling of the magnetic field of magnetospheric ring current as a function of interplanetary medium, *Space Sci. Rev.*, *59*, 83, 1992.

Foster, J. C., J. M. Holt, R. G. Musgrove, and D. S. Evans, Ionospheric convection associated with discrete levels of particle precipitation, *Geophys. Res. Lett.*, *13*, 656, 1986.

Fuller-Rowell, T. J., and D. S. Evans, Height-integrated Pedersen and Hall conductivity patterns inferred from the TIROS-NOAA satellite data, *J. Geophys. Res.*, *92*, 7606, 1987.

Gonzales, W. D., and F. S. Mozer, A quantitative model for the potential resulting from reconnection with an arbitrary interplanetary magnetic field, *J. Geophys. Res.*, *79*, 4186, 1974.

Gonzales, W. D., J. A. Joselyn, Y. Kamide, H. W. Kroehl, G. Rostoker, B. T. Tsurutani, and V. M. Vasyliunas, What is a geomagnetic storm?, *J. Geophys. Res.*, *99*, 5771, 1994.

Kamide, Y., and W. Baumjohann, Estimation of electric fields and currents from International Magnetospheric Study magnetometer data for the CDAW 6 intervals: Implications for substorm dynamics, *J. Geophys. Res.*, *90*, 1305, 1985.

Kamide, Y., and W. Baumjohann, Implications of Magnetosphere Ionosphere Coupling, in *Magnetosphere-Ionosphere Coupling*, edited by M. C. E. Huber et al., pp. 1-15, Springer-Verlag, New York, 1993.

Kamide, Y., A. D. Richmond, and S. Matsushita, Estimation of ionospheric electric fields, ionospheric currents, and field-aligned currents from ground magnetic records, *J. Geophys. Res.*, 86, 801, 1981.

Kamide, Y., and J. F. Vickery, Relative contribution of ionospheric conductivity and electric field to the auroral electrojets, *J. Geophys. Res.*, 88, 7989, 1983.

Knipp, D. J., et al., Ionospheric convection response to slow, strong variations in a northward interplanetary magnetic field: A case study for January 14, 1988, *J. Geophys. Res.*, *98*, 19,273, 1993. (Correction, *J. Geophys. Res.*, *99*, 6541, 1994.)

Kroehl, H. W., and Y. Kamide, High-latitude indices of electric and magnetic variability during the CDAW 6 intervals, *J. Geophys. Res.*, *90*, 1367, 1985.

Lu, G., A. D. Richmond, B. A. Emery, and R. G. Roble, Magnetosphere-ionosphere-thermosphere coupling: Effect of neutral winds on energy transfer and field-aligned current, *J. Geophys. Res.*, in press, 1995.

Papitashvili, V. O., B. A. Belov, D. S. Faermark, Y. I. Feldstein, S. A. Golyshev, L. I. Gromova, and A. E. Levitin, Electric potential patterns in the northern and southern polar regions parameterized by the interplanetary magnetic field, *J. Geophys. Res.*, *99*, 13,251, 1994.

Reiff, P. H., R. W. Spiro, and T. W. Hill, Dependence of polar cap potential drop on interplanetary parameters, *J. Geophys. Res.*, *86*, 7639, 1981.

Reiff, P. H., R. W. Spiro, R. A. Wolf, Y. Kamide, and J. H. King, Comparison of polar cap potential drops estimated from solar wind and ground magnetometer data: CDAW 6, *J. Geophys. Res.*, *90*, 1318, 1985.

Rich, F. J., and W. F. Denig, The major magnetic storm of March 13-14, 1989 and associated ionosphere effects, *Can. J. Phys.*, *70*, 510, 1992.

Rich, F. J., M. S. Gussenhoven, and M. E. Greenspan, Using simultaneous particle and field observations on a low altitude satellite to estimate Joule heat energy flow into the high latitude ionosphere, *Ann. Geophys., Ser. A*, *5*, 527, 1987.

Richmond, A. D., Assimilative mapping of ionospheric electrodynamics, *Adv. Space Res.*, *6*(6), 59, 1992.

Richmond, A. D., and Y. Kamide, Mapping electrodynamic features of the high-latitude ionosphere from localized observations: Technique, *J. Geophys. Res.*, *93*, 5741, 1988.

Richmond, A. D., et al., Global measures of ionospheric electrodynamic activity inferred from combined incoherent scatter radar and ground magnetometer observations, *J. Geophys. Res.*, *95*, 1061, 1990.

Robinson, R. M., R. R. Vondrak, K. Miller, T. Dabbs, and D. Hardy, On calculating ionospheric conductances from the flux and energy of precipitating electrons, *J. Geophys. Res.*, *92*, 2565, 1987.

Roble, R. G., E. C. Ridley, A. D. Richmond, and R. E. Dickinson, A coupled thermosphere/ionosphere general circulation model, *Geophys. Res. Lett.*, *15*, 1325, 1988.

Rostoker, G., Geomagnetic indices, *Rev. Geophys.*, *10*(4), 935, 1972.

Tsurutani, B. T., J. A. Slavin, Y. Kamide, R. D. Zwicki, J. H. King, and C. T. Russell, Coupling between the solar wind and the magnetosphere: CDAW 6, *J. Geophys. Res.*, *90*, 1191, 1985.

Vallance Jones, A., Historical review of great auroras, *Can. J. Phys.*, *70*, 479, 1992.

VanZandt, T. E., W. L. Clark, and J. M. Warnock, Magnetic apex coordinates: A magnetic coordinate system for the ionospheric F_2 layer, *J. Geophys. Res.*, *77*, 2406, 1972.

Vickery, J. F., R. R. Vondrak, and S. J. Matthews, Energy deposition by precipitating particles and Joule dissipation in the auroral ionosphere, *J. Geophys. Res.*, *87*, 5184, 1982.

Weimer, D. R., N. C. Maynard, W. J. Burke, and C. Liebrecht, Polar cap potentials and the auroral electrojet indices, *Planet. Space Sci.*, *38*, 1207, 1990a.

Weimer, D. R., L. A. Reinleitner, J. R. Kan, L. Zhu, and S.-I. Akasofu, Saturation of the auroral electrojet current and the polar cap potential, *J. Geophys. Res.*, *95*, 18,981, 1990b.

Wygant, J. R., R. B. Torbert, and F. S. Mozer, Comparison of S3-3 polar cap potential drops with the interplanetary magnetic field and models of magnetopause reconnection, *J. Geophys. Res.*, *88*, 5727, 1983.

C. R. Clauer and M. L. Cooper, Space Physics Research Laboratory, University of Michigan, 2455 Hayward Street, Ann Arbor, MI 48109-2143. (e-mail: clauer@pitts.sprl.umich.edu; cooper@oosik.sprl.umich.edu)

B. A. Emery and A. D. Richmond, High Altitude Observatory, National Center for Atmospheric Research, P. O. Box 3000, Boulder, CO 80307-3000. (e-mail: emery@hao.ucar.edu; richmond@hao.ucar.edu)

J. D. Winningham, Southwestern Research Institute, P. O. Drawer 28510, San Antonio, TX 78284. (e-mail: david@pemrac.space.swri.edu)

(Received January 4, 1995; revised May 1, 1995; accepted May 2, 1995.)